Journal of Thermal Analysis and Calorimetry
https://doi.org/10.1007/s10973-025-14687-7

Experimental and numerical evaluation of the cooling capacity of an earth air heat exchanger and direct evaporative cooling system with different materials and configurations over time

Nora Boultif[1] · Amar Rouag[1,2] · Yousra Boutera[3] · Müslüm Arıcı[4] · Aboubakr-Seddik Hachani[5] · Nour-El-Imane Moummi[5]

Received: 27 December 2024 / Accepted: 10 August 2025
© Akadémiai Kiadó Zrt 2025

Abstract

The present paper examines the effectiveness of two cooling systems, namely, direct evaporative cooler (DEC) and earth air heat exchanger (EAHE). Two separate models for DEC and EAHE were developed considering their special features. Both systems were analysed individually as well as combined as a hybrid system (EAHE + DEC) over time. An experimental setup of DEC system was realised to test the cooling effectiveness of three local materials (palm fibres, loofah, and eucalyptus). The two models were validated, and a high degree of agreement was observed between them and the experimental data. Results showed that palm fibres are the most efficient material among the locally studied materials, exhibiting a thermal efficiency of 70% across the various studied mass flow rates (0.236, 0.334, and 0.41 kg s^{-1}). Additionally, it was effective in reducing temperature by 9 °C. Earth air heat exchanger can effectively decrease air temperature to 29 °C but is limited in its ability to sufficiently elevate air humidity for achieving thermal comfort. For that, a case study of a hybrid system (combining EAHE and DEC systems) is presented to demonstrate their synergistic potential in the region of Biskra. The findings showed that the hybrid EAHE + DEC can provide thermal comfort in terms of temperature and humidity and reach 6 kW of cooling capacity.

Keywords Local materials · Palm fibres · Earth air heat exchanger · Direct evaporative cooling · Sustainable cooling · Arid climates

List of symbols

Symbols

C	Thermal capacity (kJ kg^{-1} K^{-1})
D	Diameter (m)
h	Convective heat transfer coefficient (W m^{-2} K^{-1})
k	Thermal conductivity (W m^{-1} K^{-1})
m	Mass (kg)
$\dot{m}$	Mass flow rate (kg s^{-1})
T	Temperature (K)
U	Overall heat transfer coefficient (W m^{-2} K^{-1})
r	Latent heat of water vaporisation (J kg^{-1})
t	Time (h)
L	Tube length (m)
ρ	Density (kg/m^3)
μ	Dynamic viscosity (Pa·s)
ω_a	Air humidity ratio ($kg_{water\ vapor}$/ $kg_{dry\ air}$)
$\omega_{a.s}$	Saturated air humidity ratio ($kg_{water\ vapor}$/ $kg_{dry\ air}$)
δ	Thickness of pad (m)

indice

a	Air
c	Convection heat transfer
db	Dry bulb
m	Convection mass transfer
p	Tube (pipe)

✉ Müslüm Arıcı
muslumarici@gmail.com

1 Laboratoire de Génie Energétique et Matériaux, LGEM, Université de Biskra, B.P.145, R.P. 07000 Biskra, Algeria

2 Faculté des Hydrocarbures, des Energies Renouvelables, des Sciences de la Terre, Département des Energies Renouvelables, Université Kasdi Merbah de Ouargla, 30 000 Ouargla, Algeria

3 Laboratoire de Génie Mécanique, LGM, Université de Biskra, B.P.145, R.P. 07000 Biskra, Algeria

4 Mechanical Engineering Department, Engineering Faculty, Kocaeli University, Umuttepe Campus, 41001 Kocaeli, Turkey

5 Département de Génie Mécanique, Université de Biskra, B.P.145, R.P. 07000 Biskra, Algeria

Published online: 27 October 2025

s	Soil
i	Inlet
o	Outlet
w	Water
wb	Wet bulb
M	Measured or experimental
N	Numerical

Acronyms

EAHE	Earth air heat exchanger
DEC	Direct evaporative cooler
Nu	Nusselt number
Pr	Prandtl number
PVC	Polyvinyl chloride
Re	Reynolds number

Introduction

In light of the challenges posed by climate change, such as extreme heatwaves associated with global warming, and in the context of increasing population growth and rising demand for buildings of various purposes, the need for cooling and ventilation systems has become more urgent than ever to ensure comfortable living conditions within these buildings. Although these systems provide an effective solution to control temperatures and humidity levels, they also contribute to exacerbating the problem of environmental pollution due to their heavy reliance on non-renewable energy and their huge electricity consumption. Therefore, addressing the environmental consequences of using these systems has become necessary by reducing consumption through the use of environmentally friendly cooling systems or integrating them with renewable energy sources.

The evaporative cooling system is one of the most important and popular alternative technologies due to its significant thermal capacity, energy saving, and simplicity. The principle of this system is to treat the air by evaporating water to cool it. Many experimental and theoretical studies have focused on studying the effectiveness of direct evaporative coolers (DECs) and the influence of different operating parameters, pad materials, and pad design on their cooling capacity. In this regard, Ahmed et al. [1] investigated three different greenhouse pad materials, including celdek, straw, and sliced wood. According to the findings, sliced wood pads performed better than alternative evaporative cooling materials. Doğramacı et al.[2] used eucalyptus fibres, which were able to lower the air temperature between 6.6 and 11.3°C, and have maximum cooling efficiencies in the range of 49 to 71%. Pumice stones, volcanic tuff, and greenhouse shade net were examined by Gunhan et al. [3] at four different air velocities and relative humidity (RH) levels. Consequently, it was discovered that an air velocity of 0.6 m s^{-1} is optimal for volcanic tuff pads. In a separate study, Sabri et al. [4] investigated the effectiveness of five different natural materials for evaporative cooling in hot climates. The results showed that eucalyptus fibres exhibited a temperature reduction of 8.2°C and a coefficient of performance (COP) of 40, making it the most efficient material. In contrast, other less common materials tested, such as aloe vera fibres and sheep wool, did not perform as well. Rasheed et al. [5] explored the effectiveness of three crossflow evaporative heat exchanger designs made from inexpensive materials. These included dv1 (aluminium and cotton with a zigzag airflow), dv2 (polypropylene with nonwoven fabric and a central airflow), and dv3 (polypropylene with nonwoven fabric and a lateral airflow). According to their findings, dv2 and dv3 outperformed dv1, with air temperature reductions of 7°C and 6.7°C and COPs reaching up to 4.2. Laknizi et al. [6] carried out a parametric study to examine how different factors, such as air velocity and the thickness of the cooling pad, influence system performance. They found that both increasing the pad thickness and boosting air velocity helped improve the system's cooling capacity. However, it resulted in increased water consumption and a lower coefficient of performance. These results were similar to those of Sellam et al. [7], who studied a palm fibre cooling pad. Mourad et al. [8] investigated the impact of varying the air gap width in a DEC system on its performance. By adjusting the gap from 0 to 150 mm and modifying the pad thickness, tests were conducted at air speeds ranging from 1 to 3 m s^{-1} and water flow rates of 15 to 60 L min^{-1} m^{-2}. Results showed that widening the air gap improved cooling efficiency and COP by 5–9% and 8–10%, respectively.

On the other hand, the earth air heat exchangers (EAHEs) are widely used in cooling buildings [9–12]. The principle of cooling utilising geothermal energy primarily depends on the difference in temperature between the depth of the earth and the surrounding atmosphere. Its simplicity and low cost characterise this technology compared to alternative energy sources, and it is considered a renewable energy technology that is receiving increasing attention from researchers. Boutera et al. [13, 14] studied the ability of an EAHE to improve the internal conditions of industrial buildings, where they found that this system could cover 38% of the cooling needs. In contrast, Dehina et al. [15] proposed a novel coaxial earth water–air heat exchanger in which water flows in an axial tube and air flows in an annular space. The results showed that the system provided 16% of the cooling load. Belloufi et al. [16] focused on investigating the behaviour of an EAHE in continuous operation for 71 h. The results of this experiment showed that the operating period had no appreciable effect on the outlet temperature and performance of EAHE. They also confirmed in another study [9] that the EAHE with a length of 33 m and an air velocity of 3.5 m s^{-1} could reduce the air temperature by

91%. Alikhani et al. [17] analysed the optimal tube length for EAHE based on performance over time. They found that soil thermal saturation after 6 days increases the optimal tube length by 37.9%. Ignoring this leads to a 57.9% underestimation and overestimated performance, highlighting the importance of accounting for long-term conditions in EAHE design. Kouki et al. [18] reviewed EAHE systems and found that pipe length, diameter, and airflow rate significantly affect performance, while pipe material has little impact. She noted that longer pipes and suitable backfill materials, such as sand or construction waste, improve cooling, although cost is a key factor in design choices.

Many studies have suggested integrating DEC systems with EAHE to enhance the cooling capacity of the two previous systems, thereby creating a hybrid system with high energy efficiency and low environmental impact. Bansal et al. [19, 20] are among the researchers interested in studying the performance of ground-air tunnel heat exchangers when combined with an evaporative cooling system. The results show that this integrated system significantly contributes to achieving the required cooling temperatures while reducing the length of the ground heat exchanger. In another study, Nemati et al. [21] investigated the efficiency of a hybrid system that combines an EAHE and an indirect evaporative cooler for cooling spaces. The results showed that using a hybrid system improved the cooling process while reducing water and energy consumption. The study presented by Harrouz et al. [22] reported that combining an EAHE with a DEC system delivered much better performance than using a DEC only. The hybrid setup led to savings of 41% and 33% in water consumption and electricity use, respectively. Nishad and Mangaraj [23] evaluated the efficiency of an EAHE + DEC to improve storage conditions for fruits and vegetables. They tested the effects of air velocity, water flow, and cooling pad thickness on humidity and temperature. The hybrid system lowered the air temperature by 16.8 °C and increased humidity to 70.85% at an air velocity of 4 m s^{-1} and a pad thickness of 0.150 m. Akbarpoor and Poshtiri [24] studied a hybrid cooling system that combined a meander-shaped EAHE with a DEC unit. Their results showed that this setup performed better overall, maintaining thermal comfort for heat loads of up to 4000 W. Notably, it used 60.2% less water and nearly 5% less electricity compared to a standard DEC system alone.

Previous studies have demonstrated that combining EAHE and DEC systems can be a significant step forward in cooling technology, delivering strong performance and enhanced energy efficiency. However, research exploring the impact of changing external climates during daily periods on the performance of these systems is still limited. This paper works to fill this research gap, where the novelty of this work as follows: (i) An in-depth analysis of the cooling performance of both EAHE system and DEC system, independently and as an integrated system over a continued period of time is conducted. (ii) The study highlights the utilisation of available local materials, such as palm fibre, loofah, and eucalyptus, in improving system performance, reflecting a commitment to sustainability and innovation. To achieve the study's aim, two distinct models are developed for the DEC and EAHE systems, taking into consideration their unique characteristics and interactions. Additionally, an experimental setup is explicitly realised for the DEC system, allowing for accurate data collection and validation of the DEC model. Through this research, the paper aims to highlight the untapped potential of the EAHE + DEC hybrid system for efficient cooling processes and offer insights into its capacity to ensure sustainable cooling over extended periods.

Methodology

To achieve the objectives of this study, the following steps are followed:

- A numerical model was developed to test the performance of an EAHE system over time.
- Natural materials, abundantly available locally, were selected and tested as a DEC system through field tests that tracked air temperature and humidity under operational conditions.
- After analysing the results, the best-performing natural material was compared to a commercial cooling pad under the same operational conditions.
- Modelling the combined system, which combines an EAHE system with the best-performing DEC pad, the overall air-cooling efficiency of the hybrid system compared to the individual systems was evaluated.

System description

Figure 1 illustrates a hybrid system that ingeniously combines an EAHE and a DEC. Before their integration, both the EAHE and DEC systems were studied individually, ensuring a comprehensive understanding of their functionalities and performance characteristics. In the system, the initial step involves the intake of hot and dry ambient air, which enters the EAHE's inlet. Inside the EAHE, the air undergoes a heat exchange process with the cooler underground environment, resulting in significant pre-cooling as the earth absorbs the excess heat. Subsequently, the pre-cooled air is directed to the DECS, where it encounters a direct evaporative cooling process. Through the interaction with water, the air experiences a remarkable temperature drop as the sensible heat is utilised for evaporating the water.

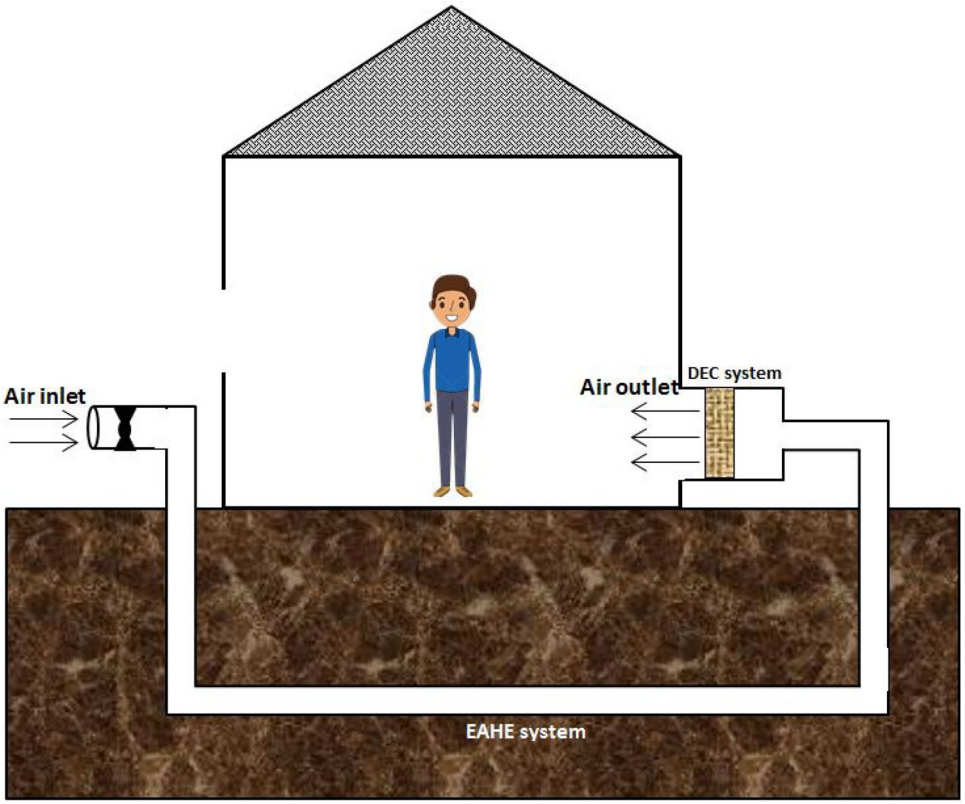


Fig. 1 Descriptive scheme of the proposed EAHE-DEC system

DEC system

Experimental study The experimental preparation is divided into two main parts: the establishment of the experimental structure and the preparation of cooling pads, which consist of natural materials available in the region, to achieve a sustainable and eco-friendly cooling system.

The experimental structure consists of a rectangular glass channel with a length of 1 m and a square cross-section of 0.09 m^2. The channel is insulated with a layer of polystyrene, 0.02 m thick, as shown in Fig. 2. The system is equipped with several components to ensure a comprehensive monitoring of the data: (1) The controller regulates system operation and manages electrical inputs to the devices; (2) The pump (HANYU B20-6) circulates water throughout the system; (3) The tank serves as a reservoir for the water used in the evaporation process, allowing for collection and reuse; (4) The exhaust fan (L300) drives airflow through the channel at controlled flow rates; (5) The digital temperature panel (TP3) measures the water temperature; (6) The water spray system keeps the cooling pads moist; (7) The DHT-22 sensor records air temperature and relative humidity at the inlet and outlet; (8) The Arduino board collects sensor data and manages system automation; and (9) The valves control water flow within the setup.

On the other hand, to study the effect of cooling pad materials on the DEC performance, three cooling pads were prepared with dimensions of 0.26×0.21 m^2, each of which consisted of several thin layers of natural fibres such as palm fibres, loofah, and eucalyptus with a thickness of 0.03 m (Fig. 3).

Numerical study This section presents the mathematical model, implemented and solved using MATLAB, to calculate the temperature and humidity variation along a commercial DEC (GLASdek7090) by analysing the heat and mass transfer under the following assumptions.

1. Air and water thermal properties are constant.
2. The pad material is homogeneous and wet uniformly and thoroughly.
3. The interface temperature of the water–air is uniform and constant.
4. The heat and mass transfer coefficients of moist air at the water surface are constant.
5. Lewis number is $Le = 1$.
6. The heat flux transfers through the surrounding are neglected.
7. The air near the water–air interface is saturated, and its temperature is equivalent to the sprinkled water temperature.

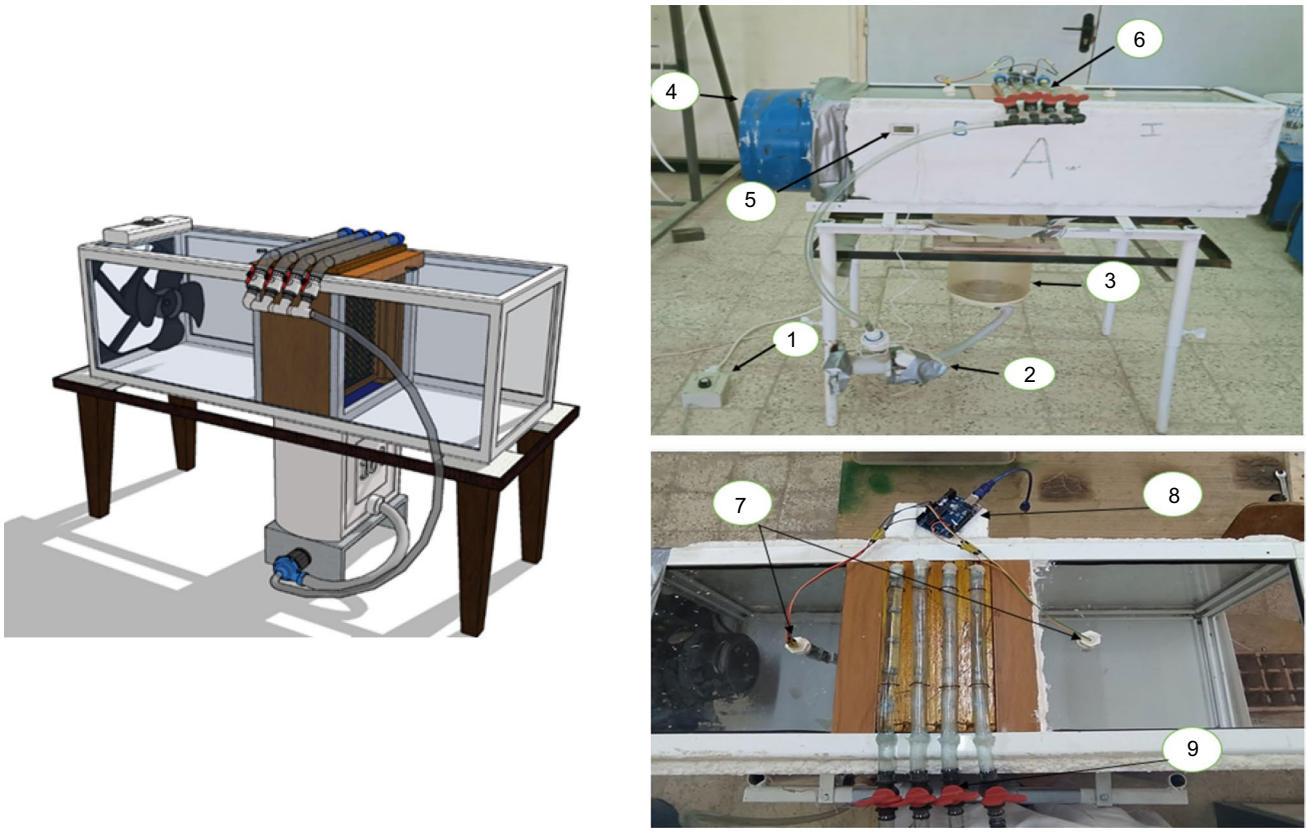


Fig. 2. 3D design and a real picture of the DEC system

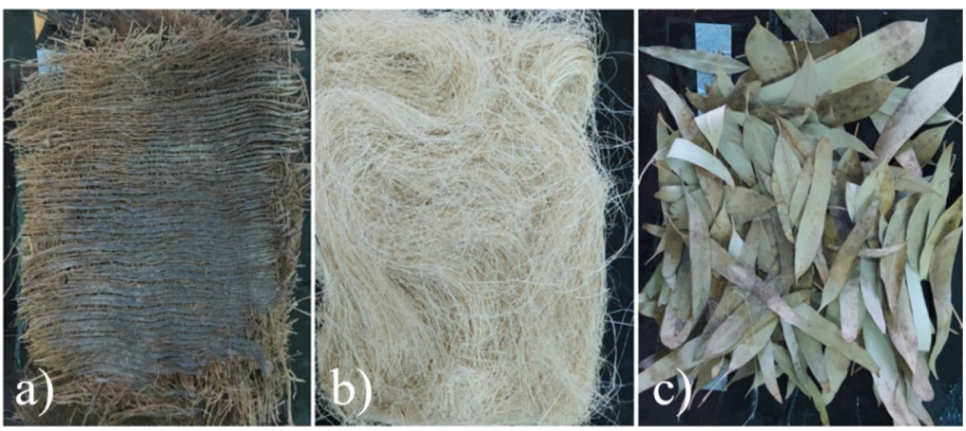


Fig. 3 The natural materials used as a cooling pad: **a** palm fibres, **b** loofah, and **c** eucalyptus

8. The air temperature and humidity change only in the x direction.

The equation given below describes the sensitive heat transfer from the air through the cooling pad due to the temperature difference:

$$d\varphi_s = h_c\left(T_{db} - T_w\right)dS = -\dot{m}_a c_p dT_{db} \quad (1)$$

The area gradient dS (m^2) is given as follows:

$$dS = \xi WH dx \quad (2)$$

where ξ is the wetted porous surface area of the pad (m^2 m^{-3}), W is the pad width (m), and H is the pad height (m).

Therefore, Eq. (1) can be written as:

$$\int_{T_{db,i}}^{T_{db,o}} \frac{1}{(T_{db} - T_w)} dT_{db} = -\frac{h_c \xi WH}{\dot{m}_a c_p} \int_0^{\delta} dx \tag{3}$$

After integration and simplification, the air temperature variation along the DEC thickness can be obtained as follows:

$$T_{db,o} = T_w + (T_{db,i} - T_w) \exp\left(-\frac{h_c \xi WH}{\dot{m}_a c_p}\right) \tag{4}$$

On the other hand, the air latent heat gain is determined as follows:

$$d\varphi_l = r\dot{m}_a d\omega_a = rh_m(\omega_{a,s} - \omega_a) dS \tag{5}$$

This equation can be written as:

$$\int_{\omega_{a,i}}^{\omega_{a,o}} \frac{1}{(\omega_a - \omega_{a,s})} d\omega_a = -\frac{h_m \xi WH}{\dot{m}_a} \int_0^{\delta} dx \tag{6}$$

Taking into consideration the assumption that the sensitive heat is equal to the latent heat, and after the integration, the air humidity variation along the DEC thickness can be calculated by [25]:

$$\omega_a = \omega_{a,s} - \frac{c_p}{r}(T_{db,i} - T_w) \exp\left(-\frac{h_c \xi WH}{\dot{m}_a c_p}\right) \tag{7}$$

The saturation efficiency of the DEC system is calculated by:

$$\varepsilon = \frac{T_i - T_o}{T_i - T_s} \times 100 \tag{8}$$

where T_i, T_o, and T_s are the inlet air-dry bulb temperature (°C), the outlet air-dry bulb temperature (°C), and the outlet air-wet bulb temperature (°C), respectively. The cooling capacity of the DEC is given by:

$$Q_c = \dot{m}_a c_p (T_i - T_o) \tag{9}$$

where $\dot{m}_a$ is the mass airflow rate (kg s^{-1}).

Earth air heat exchanger

The following assumptions were made in the development of the EAHE model and implemented using MATLAB programme:

1. The air is well mixed within the tube, without temperature stratification, and the airflow is one-dimensional and uniform along the entire length of the buried pipes.
2. The soil surrounding the heat exchanger is homogeneous.
3. The soil properties are uniform, and there is perfect contact between the soil and the pipe.
4. The air is incompressible, and its thermophysical properties remain constant.
5. Both the tube and the soil are divided into multiple layers of equal length (1 m) arranged one after another.
6. Within each layer, it is assumed that there is a constant heat exchange between the air and soil during each time step.

As shown in Fig. 4, each layer has a thickness of dx with a uniform temperature for the disturbed air, pipes, and soil. The energy balance of the layer is expressed as follows [26]:

For the air inside the tube [11]

$$\dot{m}_o C_p \frac{dT^j}{dx} = -(\pi D_i) U_{a.p} (T_a^j - T_p^j) \tag{10}$$

For the tube

$$M_P C_p \frac{dT_p}{dt} = (\pi D_i \Delta x) U_{a.p} (T_a - T_p) - (\pi D_0 \Delta x) U_{a.p} (T_a - T_s) \tag{11}$$

where

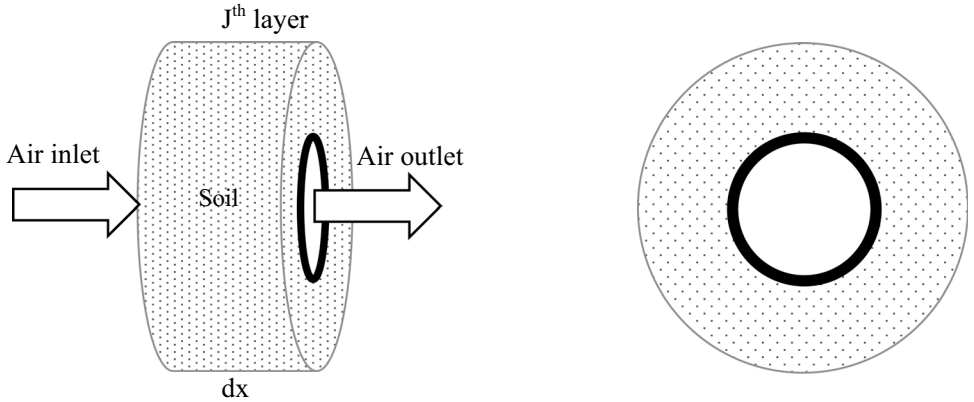


Fig. 4 Scheme of the modelled EAHE

$$M_{\mathrm{P}} = \rho_{\mathrm{p}}\left[\frac{\pi}{4}\left(D_0^2 - D_{\mathrm{i}}^2\right)\Delta x\right] \tag{12}$$

For the disturbed soil

$$M_{\mathrm{s}}C_{\mathrm{s}}\frac{\mathrm{d}T_{\mathrm{s}}}{\mathrm{d}t} = \left(\pi D_0 \Delta x\right)U_{\mathrm{ps}}\left(T_{\mathrm{p}} - T_{\mathrm{s}}\right) - \left(\pi D_{\mathrm{s}}\Delta x\right)U_{\mathrm{soil}}\left(T_{\mathrm{s}} - T_{\mathrm{soil}}\right) \tag{13}$$

where

$$M_{\mathrm{s}} = \rho_{\mathrm{s}}\left[\frac{\pi}{4}\left(D_{\mathrm{s}}^2 - D_0^2\right)\Delta x\right] \tag{14}$$

The previous differential equations of the disturbed air, tubes, and soil are discretised within a computational domain to calculate the temperature using the finite difference method [9].

For the air:

$$T_{\mathrm{a}}^{\mathrm{j}+1} = (1 - \mathrm{N})T_{\mathrm{a}}^{\mathrm{j}} + \mathrm{N}T_{\mathrm{p}}^{\mathrm{j}} \tag{15}$$

where

$$N = \frac{\left(\pi D_{\mathrm{i}}\right)U_{\mathrm{a.p}}}{\dot{m}_{\mathrm{a}}C_{\mathrm{a}}} \tag{16}$$

For the tube:

$$T_{\mathrm{p}}^{t+1} = \mathrm{A}T_{\mathrm{a}}^{\mathrm{t}} - (\mathrm{A} + \mathrm{B} - 1)T_{\mathrm{p}}^{t} + \mathrm{B}T_{\mathrm{s}}^{\mathrm{t}} \tag{17}$$

where

$$A = \frac{\left(4D_{\mathrm{i}}\right)U_{\mathrm{a,p}}\mathrm{d}t}{\rho_{\mathrm{p}}C_{\mathrm{p}}\left(D_{\mathrm{o}}^2 - D_{\mathrm{i}}^2\right)} \text{and} B = \frac{\left(4D_o\right)U_{\mathrm{p,s}}\mathrm{d}t}{\rho_{\mathrm{p}}C_{\mathrm{p}}\left(D_o^2 - D_{\mathrm{i}}^2\right)} \tag{18}$$

For the disturbed soil:

$$T_{\mathrm{s}}^{\mathrm{t}+1} = \mathrm{E}T_{\mathrm{P}}^{\mathrm{t}} - (\mathrm{E} + \mathrm{F} - 1)T_{\mathrm{s}}^{\mathrm{t}} + \mathrm{F}T_{\mathrm{soil}} \tag{19}$$

where

$$E = \frac{\left(4D_0\right)U_{\mathrm{ps}}dt}{\rho_{\mathrm{s}}C_{\mathrm{s}}\left(D_{\mathrm{s}}^2 - D_0^2\right)} \text{and} F = \frac{\left(4D_0\right)U_{\mathrm{s}}dt}{\rho_{\mathrm{s}}C_{\mathrm{s}}\left(D_{\mathrm{s}}^2 - D_0^2\right)} \tag{20}$$

The airflow rate can be evaluated as:

$$\dot{m} = \rho v_{\mathrm{a}}\left(\frac{\pi D_{\mathrm{i}}^2}{4}\right) \tag{21}$$

The heat transfer coefficient by convection between the circulating air and the buried tube is simply defined as [26]:

$$h = \frac{NuK}{D} \tag{22}$$

The Nusselt number for the flow inside a cooling tube is given by [11]:

$$Nu = 0.023Re^{0.8}Pr^{0.3} \tag{23}$$

where the Reynolds number (Re) is equal to:

$$\mathrm{Re} = \frac{\rho v_{\mathrm{a}}D_{\mathrm{i}}}{\mu} \tag{24}$$

The overall heat transfer coefficient between the circulating air and the tube is given by:

$$U_{\mathrm{a,p}} = \frac{1}{\frac{1}{h} + \frac{D_{\mathrm{i}}}{2K_{\mathrm{p}}}\log\left(\frac{D_{\mathrm{o}}+D_{\mathrm{i}}}{2D_{\mathrm{i}}}\right)} \tag{25}$$

The overall heat transfer coefficient between the buried tube and the disturbed soil is calculated as follows:

$$U_{\mathrm{a,p}} = \frac{1}{\frac{D_{\mathrm{i}}}{2K_{\mathrm{p}}}\log\left(\frac{2D_{\mathrm{o}}}{D_{\mathrm{o}}+D_{\mathrm{i}}}\right) + \frac{D_{\mathrm{o}}}{2K_{\mathrm{s}}}\log\left(\frac{D_{\mathrm{s}}+D_{\mathrm{o}}}{2D_{\mathrm{o}}}\right)}. \tag{26}$$

The conductive heat transfer coefficient between the undisturbed soil and the disturbed soil is given by:

$$U_{\mathrm{a,p}} = \frac{1}{\frac{D_{\mathrm{s}}}{2K_{\mathrm{s}}}\log\left(\frac{2D_{\mathrm{s}}}{D_{\mathrm{s}}+D_{\mathrm{o}}}\right)} \tag{27}$$

Validations

To ensure the accuracy of the developed models, both codes of the EAHE and DEC systems were validated against experimental data in the literature. Firstly, to validate the numerical code of the EAHE system, we have compared the results obtained by our code with those of Mehdid et al. [27] using the same geometrical and thermophysical parameters for a continuous operating duration of six hours. The specific parameters and characteristics of the EAHE tested by Mehdid et al. [27] are summarised in Table 1.

Figure 5 shows the comparison between the EAHE numerical model and the experimental study conducted by Mehdid et al. [27] on EAHE. The calculated air temperatures inside the EAHE exhibit a good agreement with the experimental results. The maximum deviation between numerical predictions and experimental results was found to be only 5%, demonstrating the high precision and validity of the code.

On the other hand, to verify the mathematical model presented for calculating air temperature and humidity variation along the DEC, the results obtained through this model have been compared with the experimental and numerical findings of Wu et al.[25] and Fouda and Melikyan [28], respectively, as shown in Table 2.

Table 1 Parameters and specific characteristics of the EAHE tested by Mehdid et al. [27]

Parameter	Value
Horizontal length of PVC	47 m
Inner diameter of PVC	0.11 m
Thickness of PVC	0.005 m
Depth of PVC	3 m
Air velocity	3.5 m s^{-1}
Density of air	1.225 kg m^{-3}
Density of soil	1800 kg m^{-3}
Density of PVC	1380 kg m^{-3}
Specific heat capacity of air	1005 J kg^{-1} K^{-1}
Specific heat capacity of soil	1340 J kg^{-1} K^{-1}
Specific heat capacity of PVC	900 J kg^{-1} K^{-1}
Thermal conductivity of air	0.0242 W m^{-1} K^{-1}
Thermal conductivity of soil	1.5 W m^{-1} K^{-1}
Thermal conductivity of PVC	0.16 W m^{-1} K^{-1}

According to Table 2, the maximum temperature difference between the present paper's numerical results and the experimental measurements of Wu et al. [25] is 0.41 °C and 0.01 °C, respectively, compared to the numerical results of the same reference. In addition, the predicted outlet dry bulb temperatures ($T_{N,db,o}$) by the present model exhibit better agreement with the experimental data of Wu et al. [25] compared to the numerical values provided by Fouda and Melikyan [28]. On the other hand, in terms of outlet humidity ratio $H_{N,o}$, there was a maximum difference of 1.4 g kg^{-1} when compared to the results of Fouda and Melikyan [28].

Results and discussion

In the sections, the parameters listed in Table 3 have been used as the simulation inputs for the EAHE code. For the DEC system, the input parameters for both the experiment

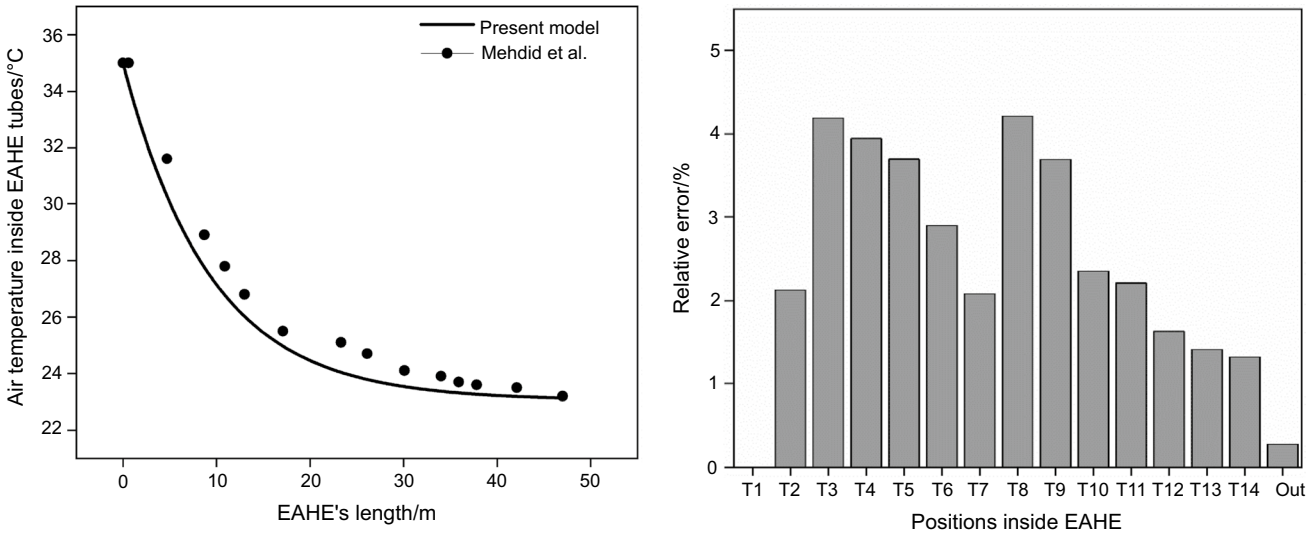


Fig. 5 Validation of the present model against Mehdid et al. [27] experimental measurements

Table 2 Temperature and humidity values of the experimental and numerical studies of [25, 28], and the present paper

Wu et al.[25]				Fouda and Melikyan [28]		Present paper	
Exp		Num		Num		Num	
$T_{db,i}$ /°C	T_{wb} /°C	$T_{M,db,o}$ /°C	$T_{N,db,o}$ /°C	$T_{N,db,o}$ /°C	$H_{N,o}$ /g/kg	$T_{N,db,o}$ /°C	$H_{N,o}$ /g kg^{-1}
27.21	20.15	22.90	22.76	22	13.8	22.77	13.6
27.84	19.06	22.66	22.32	21.5	12.8	22.32	12.4
28.54	20.55	23.50	23.51	22.5	14.5	23.52	13.9
30.5	18.86	22.77	23.18	22.15	12.35	23.18	11.7
33.09	21.69	25.49	25.92	25	16	25.92	14.4
35.01	20.36	25.90	25.80	25.2	12.8	25.80	12.6
37.06	23.42	28.01	28.48	27.8	16.5	28.48	15.8

Table 3 Simulation Inputs for the EAHE System

Parameter (unit)	Value
Ambient temperature /°C	36
Soil temperature °C	22
Air velocity /m s^{-1}	6.13
Mass flow rate kg s^{-1}	0.41
Pipe length /m	50
Inner pipe diameter /m	0.2636
Thickness of the pipe m	0.005

and the simulation are provided in Tables 4 and 5, respectively. In these tables, the input parameters are represented by $T_{db,i}$ (°C), T_w (°C), and RH_i (%), where "i" refers to the input values for the dry bulb temperature, wet bulb temperature, and relative humidity.

In order to demonstrate the EAHE's capability in efficiently reducing the temperature of the incoming air, Fig. 6 is plotted, which illustrates the temporal evolution of air temperature inside the EAHE, utilising the inlet temperatures provided in Table 4a for an air mass flow rate of 0.41 kg s^{-1} and a pipe diameter of 0.26 m. From Fig. 6, EAHE proves to be highly effective in its temperature reduction process. The air temperature within the heat exchanger experiences a noticeable decline as a function of time. This decline is a result of the heat exchange process between the air and the surrounding soil. A key observation from Fig. 6 is that the length of the tubes plays a significant role in determining the efficiency of the EAHE. Notably, when the pipe length is relatively large, the temperature of the air inside the EAHE reaches lower values.

Figure 7 demonstrates that as the air moves through the pipe, the temperature decreases gradually. In the early sections of the pipe (from 0 to 10 m), the air temperature experiences a significant drop due to the high temperature gradient between the hot incoming air and the cooler surrounding soil. However, as the air continues to travel through the pipe, the temperature reduction becomes less pronounced, particularly in the last sections (near 40–50 m). This shows that while increasing the pipe length does improve the cooling effect, the rate of temperature decrease diminishes as the air temperature approaches the soil temperature, indicating that additional pipe length offers diminishing returns in cooling efficiency. In the same figure, the effect of operation time on the performance of the EAHE system is not fully apparent, as the observation period is relatively short. The system is still primarily governed by the initial temperature gradient between the air and the soil, and the cooling rate has not yet significantly slowed down. To fully understand the long-term performance of the EAHE system in real applications, an additional study addressing the effect of soil thermal saturation would be required.

Table 4 summarises the results of field measurements of dry air temperature and humidity at the duct inlet and outlet, as well as wet bulb temperature and water temperature for each cooling pad material, conducted at 5-min intervals (from May 17 to 30, 2022). These measurements were conducted at controlled airflow rates of 0.236, 0.334, and 0.410 kg s^{-1}. The results showed that palm fibres exhibited the maximum reduction in dry air temperature of 9 °C. The fibre's effectiveness was moderate, with a maximum reduction of 8 °C at airflow rates of 0.410 and 0.334 kg s^{-1}, and 7 °C at 0.236 kg s^{-1}. In contrast, eucalyptus performed poorly, with a maximum reduction of 4 °C. In light of these results, palm fibres were selected for comparison with a commercial DEC cooling pad (GLASdek 7090). To maintain the integrity and consistency of the evaluation, the same external conditions of palm fibre were used as input parameters for the numerical modelling of the commercial pad.

Table 5 presents the numerical results for the dry air temperature and humidity at the outlet of the GLASdek7090 cooling pad. The results indicated that the commercial DEC cooling pad demonstrated more stable cooling performance. Despite fluctuations in the inlet air temperature, the outlet air temperature remained nearly constant, with a maximum variation of 1.7 °C. It also achieved a maximum temperature drop of 10 °C, demonstrating superior performance compared to palm fibre.

Figure 8 shows the saturation effectiveness and cooling capacity of four different cooling pad materials (palm fibres, loofah, eucalyptus, and GLASdek7090) at airflow rates of 0.236, 0.334, and 0.410 kg s^{-1}. According to the results, the eucalyptus saturation effectiveness increases with the increase in airflow rate until it reaches a maximum value of 50%, while this value remains constant at 70.2% for the loofah, despite the increase in airflow. In contrast, an opposite effect is observed on GLASdek7090, as the lowest saturation effectiveness value (69.6%) occurs at 0.410 kg s^{-1}. Palm fibres exhibited different behaviour, as the saturation effectiveness increased with the increasing flow to a maximum value of 70.3% at 0.334 kg s^{-1}, then decreased to 67.2% at a flow of 0.410 kg s^{-1}.

Moreover, increasing the airflow showed a positive effect on improving the cooling capacity of the four pads, with the GLASdek7090 achieving the highest cooling capacity of 3955.7 W at a flow rate of 0.410 kg s^{-1}.

Figures 9a and b illustrate the impact of different cooling pad materials on the outlet air temperature and relative humidity at a constant airflow rate of 0.41 kg s^{-1}. The results indicate that the synthetic pad, GLASdek7090, delivered the highest cooling performance, achieving a temperature reduction of up to 10 °C. This was followed by palm fibre and then loofah, with decreases of 9 °C and 8 °C, respectively. Eucalyptus pillows performed the least.

Table 4 The measured parameters of the three experimental cooling pads: a) Palm fibre, b) Loofah, and c) Eucalyptus at three different airflow rates

a) **Palm fibres**

	$\dot{m}_{a,1}$ = 0.236 /kg/s						$\dot{m}_{a,2}$ = 0.334 /kg/s						$\dot{m}_{a,3}$ = 0.410 /kg/s					
Time step / min)	$T_{db,i}$ /°C	T_w °C	RH_i /%	T_{wb} /°C	$T_{db,o}$ /°C	RH_o /%	$T_{db,i}$ /°C	T_w /°C	RH_i /%	T_{wb} /°C	$T_{db,o}$ /°C	RH_o /%	$T_{db,i}$ /°C	T_w /°C	RH_i /%	T_{wb} /°C	$T_{db,o}$ /°C	RH_o /%
00:05	28	27.2	38	18.1	27	48	**36**	25.8	33	22.9	30	37	**35**	29.5	31	21.7	30	46
00:10	31	27.8	34	19.5	26	49	**36**	27.8	32	22.6	29	46	**36**	27.9	31	22.4	27	47
00:15	33	30.2	33	20.7	26	48	**35**	25.7	31	21.7	28	46	**34**	29.1	34	21.7	26	48
00:20	33	27.9	33	20.7	25	49	**35**	25.3	32	21.9	28	47	**36**	29.3	32	22.6	27	46
00:25	34	30.0	32	21.2	27	47	**34**	26.9	31	20.9	27	46	**35**	28.8	31	21.7	27	46
00:30	34	26.8	32	21.2	26	48	**35**	28.2	33	22.2	27	47	**36**	28.8	32	22.6	27	46
00:35	34	29.5	32	21.2	28	47	**35**	25.2	32	21.9	26	47	**35**	28.9	32	21.9	27	45
00:40	34	27.8	32	21.2	26	47	**34**	27.3	31	20.9	28	46	**36**	28.5	32	22.6	28	45
00:45	34	30.6	32	21.2	27	47	**35**	25.6	33	22.2	26	48	**36**	28.8	32	22.6	28	45
00:50	35	27.1	31	21.7	26	47	**36**	28.8	31	22.4	27	47	**35**	28.6	33	22.2	27	47
00:55	35	29.8	31	21.7	28	47	**36**	26.1	31	22.4	29	46	**35**	28.6	33	22.2	27	46
01:00	34	27.8	31	20.9	27	47	**36**	28.8	31	22.4	28	46	**36**	28.8	32	22.6	28	45
b) **Loofah**																		
	$\dot{m}_{a,1}$ = 0.236 /kg/s						$\dot{m}_{a,2}$ = 0.334 /kg/s						$\dot{m}_{a,3}$ = 0.410 /kg/s					
00:05	32	27.8	39	21.3	31	45	**31**	29.1	44	21.6	26	45	**34**	28.4	39	22.8	28	49
00:10	32	28.6	40	21.5	30	49	**31**	29.0	42	21.2	28	48	**34**	30.6	39	22.8	27	49
00:15	32	27.2	39	21.3	27	49	**32**	28.4	39	21.3	29	52	**33**	30.6	37	21.6	29	48
00:20	32	29.3	39	21.3	25	56	**32**	30.0	40	21.5	27	47	**33**	29.6	38	21.8	26	49
00:25	32	28.6	39	21.3	27	47	**32**	30.3	40	21.5	29	44	**33**	28.2	38	21.8	27	47
00:30	32	29.4	39	21.3	26	51	**32**	29.1	39	21.3	30	47	**33**	30.6	39	22.1	27	59
00:35	31	27.6	40	20.8	27	48	**32**	30.4	40	21.5	27	44	**34**	29.1	37	22.4	28	49
00:40	32	27.3	39	21.3	26	55	**32**	31.2	39	21.3	29	42	**34**	30.6	38	22.6	26	50
00:45	32	27.5	38	21.1	27	51	**33**	28.2	38	21.8	30	50	**33**	29.4	39	22.1	27	47
00:50	32	29.4	39	21.3	28	50	**33**	28.8	37	21.6	26	45	**33**	29.3	39	22.1	29	52
00:55	33	27.6	39	22.1	27	55	**34**	30.5	38	22.6	26	50	**34**	27.8	37	22.4	28	50
01:00	32	27.8	38	21.1	27	49	**33**	26.0	39	22.1	28	53	**33**	29.7	38	21.8	27	50
c) **Eucalyptus**																		
	$\dot{m}_{a,1}$ = 0.236 /kg/s						$\dot{m}_{a,2}$ = 0.334 /kg/s						$\dot{m}_{a,3}$ = 0.410 /kg/s					
00:05	33	28.7	36	21.4	30	42	**29**	28.3	40	19.2	25	49	**28**	28.0	41	20.2	28	45
00:10	33	30.1	36	21.4	30	42	**29**	29.5	40	19.2	25	48	**28**	29.4	41	20.2	28	45
00:15	33	27.7	36	21.4	30	42	**29**	28.5	41	19.4	27	46	**28**	27.0	40	20.0	28	45
00:20	33	28.6	36	21.4	30	43	**29**	27.2	41	19.4	26	47	**28**	27.6	40	20.0	27	46

Table 4 (continued)

a) **Palm fibres**

Time step / min)	$\dot{m}_{a,1}$ = 0.236 /kg/s						$\dot{m}_{a,2}$ = 0.334 /kg/s						$\dot{m}_{a,3}$ = 0.410 /kg/s					
	$T_{db,i}$ /°C	T_w °C	RH_i /%	T_{wb} /°C	$T_{db,o}$ /°C	RH_o /%	$T_{db,i}$ /°C	T_w /°C	RH_i /%	T_{wb} /°C	$T_{db,o}$ /°C	RH_o /%	$T_{db,i}$ /°C	T_w /°C	RH_i /%	T_{wb} /°C	$T_{db,o}$ /°C	RH_o /%
00:25	33	30.1	36	21.4	30	44	**29**	28.8	41	19.4	27	47	**28**	27.7	41	20.2	26	46
00:30	33	29.0	36	21.4	30	42	**29**	27.4	41	19.4	27	48	**30**	27.5	41	20.2	27	47
00:35	33	28.6	36	21.4	30	43	**30**	28.6	41	20.2	27	46	**30**	26.8	40	20.8	28	50
00:40	33	28.8	36	21.4	30	44	**30**	28.1	41	20.2	27	49	**31**	28.7	40	20.8	26	48
00:45	33	31.1	36	21.4	30	43	**29**	27.6	41	19.4	27	47	**31**	27.1	40	20.8	27	45
00:50	33	29.1	36	21.4	30	43	**30**	29.3	40	20.0	27	46	**31**	26.4	41	21.0	28	50
00:55	33	30.3	36	21.4	31	41	**30**	26.6	41	20.2	27	37	**31**	28.3	40	20.8	28	49
01:00	34	30.3	36	22.1	31	41	**30**	26.6	40	20.0	27	45	**31**	27.6	41	21.0	28	47

In terms of humidity, the GLASdek 7090 pad exhibited the highest relative humidity, ranging from 67.9 to 70.2%, whereas natural materials maintained acceptable humidity levels of 45 to 50%.

These performance differences are due to the distinct physical properties of the materials used, including their effective surface area and ability to retain water for extended periods. The commercial pad (GLASdek 7090) features a geometric structure that promotes even water distribution and enhances heat and mass transfer efficiency. In contrast, loofah features a more open fibre network that retains water moderately, allowing for relatively uniform wetting and contributing to stable but less efficient cooling performance. What enhances the performance of palm fibres is their denser, rougher texture, which improves their ability to retain water for longer periods and prevents water from flowing easily, thereby prolonging the evaporation process and improving overall cooling efficiency. On the other hand, eucalyptus exhibits a flat and loosely arranged configuration with significant spacing between them. This structural feature facilitates rapid water drainage and reduces surface wetting time, thereby limiting the interaction between water and air. As a result, the cooling performance is relatively poor, especially during the initial phase of system operation.

Moreover, these structural differences are also reflected in the resulting air humidity levels. The engineered structure of the GLASdek7090 pad supports higher evaporation rates, resulting in greater humidity levels at the outlet compared to the more limited performance of natural materials.

Case study in the hybrid EAHE + DEC

Figure 10 illustrates the evolution of outlet temperatures from the three distinct cooling systems, i.e., the EAHE, the DEC, and the hybrid EAHE + DEC system. From the results of Fig. 10, it is evident that the EAHE system maintains an outlet temperature of around 29 °C. This system exploits the relatively stable temperature of the underground to provide cooling. However, this technique has limitations in achieving lower temperatures, as it primarily relies on the earth's subsurface temperature. On the other hand, the DEC system exhibits an outlet temperature of approximately 26. °C. This cooling method employs the principle of evaporative cooling, utilising the evaporative cooling effect of water to bring down the air temperature. While more effective than the EAHE in achieving lower air temperatures, the DEC system is more affected by the ambient air conditions and humidity levels. The best findings emerge from the hybrid EAHE + DEC system, which exhibits a remarkably low outlet temperature of around 22 °C. The integration of both the EAHE and the DEC systems is highly efficient. This type of coupling (i.e., EAHE + DEC) leverages the strengths of both

Table 5 The numerical results of the commercial cooling pad, d) GLASdek7090, at three different air flow rates

d) **GLASdek7090**											
$\dot{m}_{a,1}=0.236$ /kg/s				$\dot{m}_{a,2}=0.334$ /kg/s				$\dot{m}_{a,3}=0.410$ /kg/s			
$T_{db,I}$ /°C	T_{wb}/°C	$T_{db,o}$ /°C	RH_o /%	$T_{db,i}$ /°C	T_{wb} /°C	$T_{db,o}$ /°C	RH_o /%	$T_{db,i}$ /°C	T_{wb} /°C	$T_{db,o}$ /°C/	RH_o /%
28	18.1	20.6	77.8	36	22.9	26.9	70.8	35	21.7	26.1	68.1
31	19.5	22.5	75.5	36	22.6	26.6	70.4	36	22.4	26.9	67.9
33	20.7	23.9	75.1	35	21.7	25.7	70.2	34	21.7	25.7	70.2
33	20.7	23.9	75.1	35	21.9	25.9	70.6	36	22.6	27.0	68.4
34	21.2	24.5	74.5	34	20.9	24.9	69.9	35	21.7	26.1	68.2
34	21.2	24.5	74.5	35	22.2	26.1	71.5	36	22.6	27.0	68.4
34	21.2	24.5	74.5	35	21.9	25.9	70.8	35	21.9	26.2	68.7
34	21.2	24.5	74.5	34	20.9	24.9	70.1	36	22.6	27.0	68.4
34	21.2	24.5	74.5	35	22.2	26.1	71.5	36	22.6	27.0	68.4
35	21.7	25.1	81.6	36	22.4	26.5	70.1	35	22.2	26.4	69.4
35	21.7	25.1	81.6	36	22.4	26.5	70.1	35	22.2	26.4	69.4
34	20.9	24.3	73.3	36	22.4	26.5	70.1	36	22.6	27.0	68.4

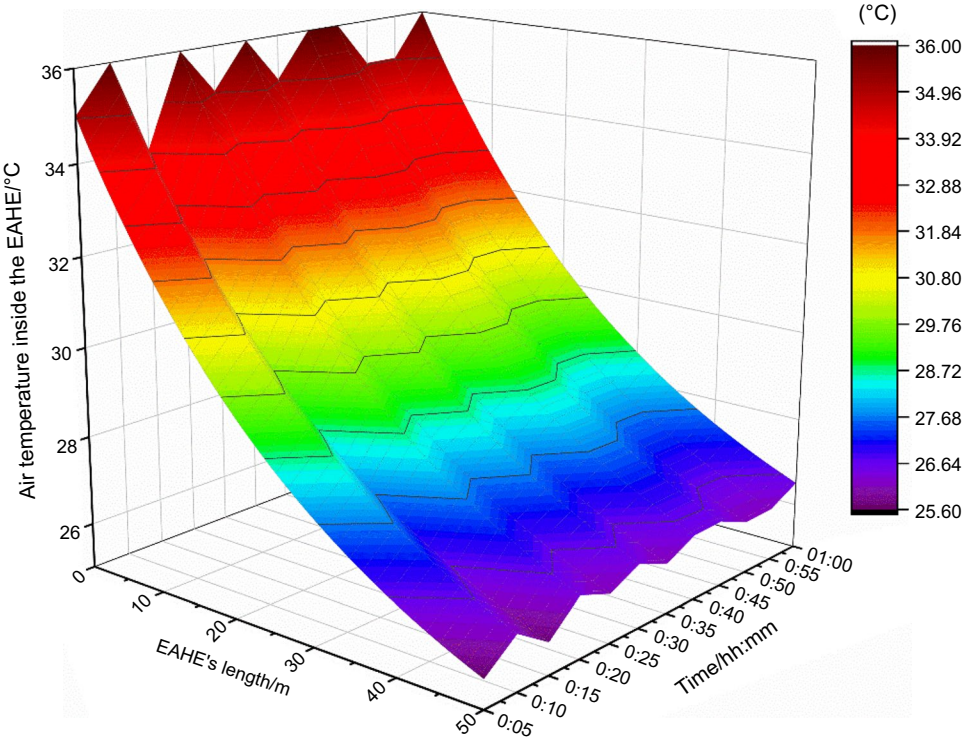


Fig. 6 Air distribution inside the EAHE

systems: the EAHE provides relatively stable pre-cooling, and the DEC offers enhanced cooling through evaporative processes. As a result, the hybrid system achieves significantly lower outlet temperatures, reaching levels that are much closer to or even within the optimal comfort range for occupants.

In the context of cooling capacity, the hybrid EAHE + DEC system demonstrated the best performance, with a maximum cooling capacity of 6 kW, as shown in Fig. 11. The EAHE system plays a crucial role in pre-cooling the air, while passage through the DEC system results in a further reduction in air temperature due to evaporation across the pad. Thus, the hybrid system achieves significantly higher cooling capacities than the individual systems.

On the other hand, the hybrid system offers significant energy efficiency improvements by relying on renewable energy sources, such as geothermal energy for the EAHE and evaporative cooling for the DEC, which reduces reliance

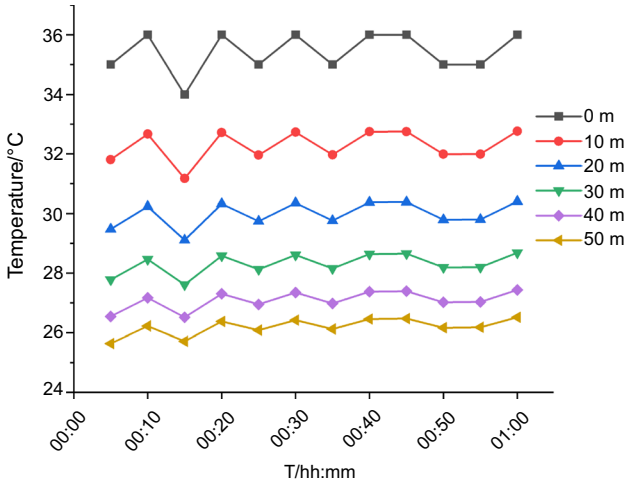


Fig. 7 Variation of air Temperature inside the EAHE as a function of time at different Pipe Locations

on energy-intensive compressors used in conventional AC units. This results in lower operational costs, despite higher initial installation costs for infrastructure. Furthermore, the hybrid system has a much lower environmental impact, producing negligible emissions compared to the high carbon footprint of conventional AC systems that rely on electricity and refrigerants. The use of local materials in the DEC system further reduces material costs and supports sustainability. Therefore, conducting a detailed comparison with conventional air-conditioning systems would better illustrate the advantages of the hybrid system, especially in terms of energy efficiency, lifecycle costs, and environmental impact.

Scaling up the EAHE + DEC hybrid system to full-size residential or commercial buildings introduces challenges related to increased airflow and cooling capacity requirements. The system would need larger cooling pads and extended EAHE pipe lengths to meet these demands. In urban environments, space limitations may require the use

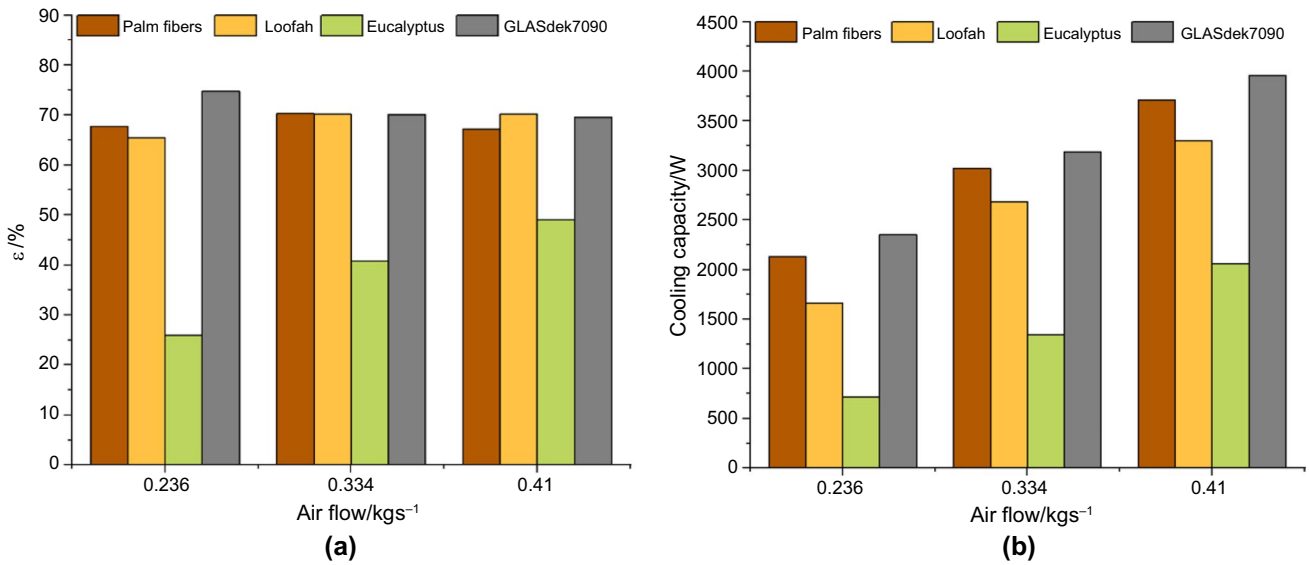


Fig. 8 **a** The saturation effectiveness and **b** the cooling capacity of four different pad materials at three air flow rates

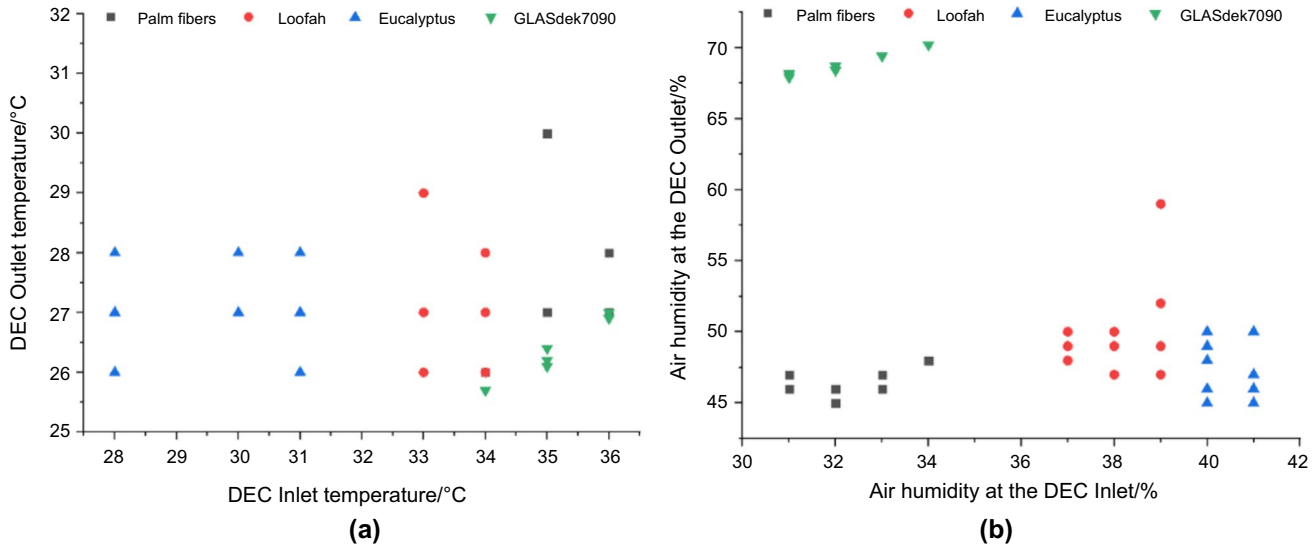


Fig. 9 **a** The air temperature and **b** humidity of the four different cooling pad materials

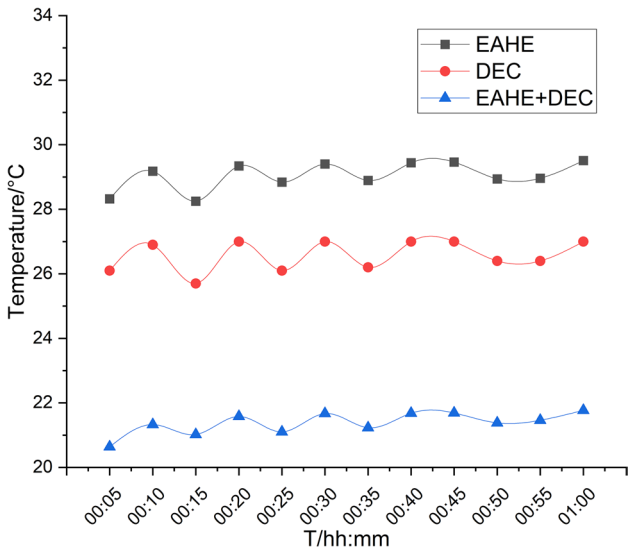


Fig. 10 Outlet temperatures from EAHE, DEC, and EAHE + DEC systems over time

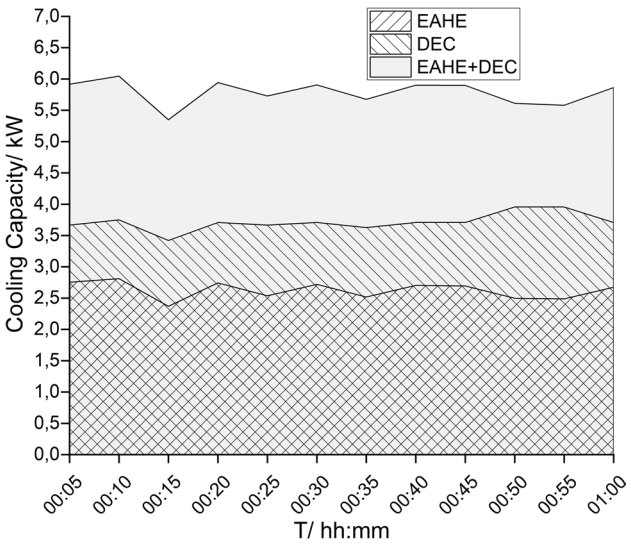


Fig. 11 EAHE, DEC and EAHE + DEC systems' cooling capacities over time

of vertical or coaxial EAHE systems. Additionally, retrofitting existing buildings would involve modifications to the infrastructure, including ventilation and water distribution systems. Sophisticated control mechanisms, including automated systems to optimise the performance of both DEC and EAHE, would also be needed. These challenges can be addressed by modular system designs, integration with renewable energy sources, and further research on system adaptability in larger-scale applications.

Conclusion

This paper evaluated the cooling efficiency of a direct evaporative cooler (DEC) system and an earth air heat exchanger (EAHE) system in a hot and dry climate such as Biskra region, Algeria. The test not only examined the performance of EAHE and DEC separately, but also evaluated the performance of a hybrid system (EAHE + DEC). Two numerical models were developed for each system and validated with experimental data to ensure the accuracy of the results. Furthermore, three local materials (eucalyptus, loofah, and palm

fibre) were experimentally tested for use as environmentally friendly DEC systems. Finally, the most effective of these materials was compared with the commercial GLASdek 7090 in terms of cooling capacity, efficiency, and outlet temperature under the same experimental conditions.

The study highlighted that the GLASdek7090 pad demonstrated the highest cooling potential, reducing temperatures by up to 9.1 °C. However, palm fibres and loofah also proved effective, lowering temperatures by 9 °C and 8°C, respectively. However, eucalyptus had a minimal impact on air temperature, particularly during the initial cooling period from 5 to 15 min. In terms of thermal efficiency, palm fibres are the most efficient material compared to the other studied local materials, achieving a thermal efficiency of 70% at different mass flow rates (0.236, 0.334, and 0.41 kg s^{-1}). In addition, it was observed that both thermal efficiency and cooling capacity improved with higher air mass flow rates.

On the other hand, although EAHE has demonstrated the ability to reduce air temperature, its capacity to increase humidity and achieve thermal comfort remains limited. In this regard, a hybrid system combining EAHE and DEC was presented as a viable solution to leverage their synergistic potential within the Biskra climate. By integrating the strengths of both technologies, the hybrid EAHE + DEC system has optimised cooling efficiency. EAHE contributes to maintaining air temperatures at around 29°C through underground cooling, while DEC enhances the process by cooling air to approximately 26.5°C through water evaporation, despite being influenced by external temperatures. By leveraging EAHE's stability and DEC's evaporation, EAHE + DEC yields encouraging results, with an outlet temperature of approximately 22 °C and a cooling capacity of 6 kW.

In future work, it is essential to consider transient conditions, such as fluctuating outdoor temperatures and humidity, to fully understand the dynamic performance of the hybrid EAHE + DEC system. By incorporating these variations into the modelling process, it can be better assessed how the system responds to real-world environmental changes and improve its adaptability for different climatic conditions.

Acknowledgements This study was supported by the General Directorate of Scientific Research and Technological Development (DGRSDT) of the Algerian Ministry of Higher Education and Scientific Research as a part of PRFU project A11N01UN300120230002.

References

1. Ahmed EM, Abaas O, Ahmed M, Ismail MR. Performance evaluation of three different types of local evaporative cooling pads in greenhouses in Sudan. Saudi J Biol Sci. 2011;18(1):45–51. https://doi.org/10.1016/j.sjbs.2010.09.005
2. Doğramacı PA, Riffat S, Gan G, Aydın D. Experimental study of the potential of eucalyptus fibres for evaporative cooling. Renew Energy. 2019;131:250–60. https://doi.org/10.1016/j.renene.2018.07.005
3. Gunhan T, Demir V, Yagcioglu A. Evaluation of the suitability of some local materials as cooling pads. Biosyst Eng. 2007;96(3):369–77. https://doi.org/10.1016/j.biosystemseng.2006.12.001
4. Sabri S, et al. Experimental performance study of five natural pads for direct evaporative cooling. Energy Build. 2025. https://doi.org/10.1016/j.enbuild.2025.116046.
5. Rasheed S, et al. Enhanced thermal efficiency in crossflow evaporative cooling systems: a comparative study of materials and flow patterns. Int Commun Heat Mass Transfer. 2025;167:109252. https://doi.org/10.1016/j.icheatmasstransfer.2025.109252
6. Laknizi A, Mahdaoui M, Abdellah AB, Anoune K, Bakhouya M, Ezbakhe H. Performance analysis and optimal parameters of a direct evaporative pad cooling system under the climate conditions of Morocco. Case Stud Therm Eng. 2019;13:100362. https://doi.org/10.1016/j.csite.2018.11.013
7. Sellam S-H, et al. Experimental performance evaluation of date palm fibers for a direct evaporative cooler operating in hot and arid climate. Case Stud Therm Eng. 2022;35: 102119. https://doi.org/10.1016/j.csite.2022.102119
8. Mourad AM, El Moghazy IM, Hassan AA. Experimental investigation of a direct evaporative cooling system considering the effect of air gap spacing between pads. Appl Therm Eng. 2025;262:125205. https://doi.org/10.1016/j.applthermaleng.2024.125205
9. Belloufi Y, et al. Transient assessment of an earth air heat exchanger in warm climatic conditions. Geothermics. 2022;104:102442. https://doi.org/10.1016/j.geothermics.2022.102442
10. Rouag A, Benchabane A, Mehdid C-E. Thermal design of Earth-to-Air Heat Exchanger. Part I a new transient semi-analytical model for determining soil temperature. J Clean Prod. 2018;182:538–44. https://doi.org/10.1016/j.jclepro.2018.02.089.
11. Rouag A, et al. Technical solution for malfunction of air coolers and condensers in hot climates: thermal design of a Geothermal Air-Cooler. Energy Sources, Part A: Recov Utilis Environ Effects. 2020;2020:1–14. https://doi.org/10.1080/15567036.2020.1777225
12. Boutera Y, et al. A parametric analysis of the earth air heat exchangers' thermal efficiency and their effect on surrounding soil over time. J Appl Eng Sci Technol. 2025;5(1):111. https://doi.org/10.69717/jaest.v5.i1.111.
13. Boutera Y, Boultif N, Rouag A, Beldjani C, Moummi N. Performance of earth-air heat exchanger in cooling, heating, and reducing carbon emissions of an industrial poultry farm: a case study. Energy Sources Part A Recover Util Environ Eff. 2022;44(4):9564–83. https://doi.org/10.1080/15567036.2022.2132323.
14. Boutera Y, et al. Evaluation of the earth-air heat exchanger's performance in improving the indoor conditions of an industrial poultry house using computational fluid dynamics verified with field tests. J Clean Prod. 2024;434: 140218. https://doi.org/10.1016/j.jclepro.2023.140218.
15. Dehina K, Mokhtari AM, Souyri B. Energy modelling of a new co-current coaxial earth–water to air-heat exchanger. Case study: heating of house in Biskra-Algeria. Geothermics. 2020;87:101836. https://doi.org/10.1016/j.geothermics.2020.101836
16. Belloufi Y, et al. Numerical and experimental investigation on the transient behavior of an earth air heat exchanger in continuous operation mode. Int J Heat Technol. 2017;35(2):279–88. https://doi.org/10.18280/ijht.350208.
17. Alikhani A, Maerefat M, Sobhani SMJ. Analytical investigation on the optimal tube length of Earth-to-Air heat exchanger (EAHE).

Geothermics. 2025;127: 103250. https://doi.org/10.1016/j.geothermics.2025.103250
18. Kouki N, D'Agostino D, Vityi A. Properties of Earth-to-Air heat exchangers (EAHE): insights and perspectives based on system performance. Energies. 2025;18(7):1759. https://doi.org/10.3390/en18071759
19. Bansal V, Mathur J. Performance enhancement of earth air tunnel heat exchanger using evaporative cooling. Int J Low-Carbon Technol. 2009;4(3):150–8. https://doi.org/10.1093/ijlct/ctp017
20. Bansal V, Mishra R, Agarwal GD, Mathur J. Performance analysis of integrated earth–air-tunnel-evaporative cooling system in hot and dry climate. Energy Build. 2012;47:525–32. https://doi.org/10.1016/j.enbuild.2011.12.024
21. Nemati N, Omidvar A, Rosti B. Performance evaluation of a novel hybrid cooling system combining indirect evaporative cooler and earth-air heat exchanger. Energy. 2021;215: 119216. https://doi.org/10.1016/j.energy.2020.119216
22. Harrouz JP, Al Assaad D, Orabi M, Ghali K, Ouahrani D, Ghaddar N. Modeling and optimisation of poultry house passive cooling strategies in semiarid climates. Int J Energy Res. 2021;45(15):20795–811. https://doi.org/10.1002/er.7139
23. Barakat S, Ramzy A, Hamed A, El Emam S. Enhancement of gas turbine power output using earth to air heat exchanger (EAHE) cooling system. Energy Convers Manage. 2016;111:137–46. https://doi.org/10.1016/j.enconman.2015.12.060
24. Akbarpoor AM, Poshtiri AH. Cooling urban buildings with a combined meander EAHE–DEC system: energy and water consumption analysis. J Build Eng. 2025;108: 112850. https://doi.org/10.1016/j.jobe.2025.112850
25. Wu J, Huang X, Zhang H. Theoretical analysis on heat and mass transfer in a direct evaporative cooler. Appl Therm Eng. 2009;29(5–6):980–4. https://doi.org/10.1016/j.applthermaleng.2008.05.016
26. Kheireddine M-A, et al. Adaptation of adsorption cooling system for hot and dry climates: use of ground water heat exchanger coupled to direct evaporative cooling tower. Energy Sources Part A Recover Util Environ Eff. 2023;45(3):9133–48. https://doi.org/10.1080/15567036.2023.2231883
27. Mehdid C-E, et al. Thermal design of Earth-to-air heat exchanger. Part II a new transient semi-analytical model and experimental validation for estimating air temperature. J Clean Prod. 2018;198:1536–44. https://doi.org/10.1016/j.jclepro.2018.07.063.
28. Fouda A, Melikyan Z. A simplified model for analysis of heat and mass transfer in a direct evaporative cooler. Appl Therm Eng. 2011;31(5):932–6. https://doi.org/10.1016/j.applthermaleng.2010.11.016

Publisher's Note Springer Nature remains neutral with regard to jurisdictional claims in published maps and institutional affiliations.

Springer Nature or its licensor (e.g. a society or other partner) holds exclusive rights to this article under a publishing agreement with the author(s) or other rightsholder(s); author self-archiving of the accepted manuscript version of this article is solely governed by the terms of such publishing agreement and applicable law.